MITSUBISHI ELECTRIC RESEARCH LABORATORIES
http://www.merl.com

Inverse Multiple Scattering With Phaseless Measurements

Ma, Yanting; Lodhi, Muhammad Asad; Mansour, Hassan; Boufounos, Petros T.; Liu, Dehong

TR2020-041 April 11, 2020

Abstract

We study the problem of reconstructing an object from phaseless measurements in the context of inverse multiple scattering. Our formulation explicitly decouples the variables that represent the unknown object image and the unknown phase, respectively, in the forward model. This enables us to simultaneously optimize over both unknowns with appropriate regularization for each. The resulting optimization problem is nonconvex due to the nonlinear propagation model for multiple scattering and the nonconvex regularization of the phase variables. Nevertheless, we demonstrate experimentally that we can solve the optimization problem using a variation of the fast iterative shrinkage-thresholding algorithm (FISTA)—a convex algorithm, popular for its speed and simplicity—that converges well in our experiments. Numerical results with both simulated and experimentally measured data show that the proposed method outperforms the state-ofthe-art phaseless inverse scattering method.

IEEE International Conference on Acoustics, Speech, and Signal Processing (ICASSP)

INVERSE MULTIPLE SCATTERING WITH PHASELESS MEASUREMENTS

Muhammad Asad Lodhi[1]*, Yanting Ma*[2]*, Hassan Mansour*[2]*, Petros T. Boufounos*[2]*, and Dehong Liu*[2]

[1] Rutgers University, Dept. of Elec. and Comp. Engineering, New Brunswick, NJ, USA
[2] Mitsubishi Electric Research Laboratories, Cambridge, MA, USA

ABSTRACT

We study the problem of reconstructing an object from phaseless measurements in the context of inverse multiple scattering. Our formulation explicitly decouples the variables that represent the unknown object image and the unknown phase, respectively, in the forward model. This enables us to simultaneously optimize over both unknowns with appropriate regularization for each. The resulting optimization problem is nonconvex due to the nonlinear propagation model for multiple scattering and the nonconvex regularization of the phase variables. Nevertheless, we demonstrate experimentally that we can solve the optimization problem using a variation of the fast iterative shrinkage-thresholding algorithm (FISTA)—a convex algorithm, popular for its speed and simplicity—that converges well in our experiments. Numerical results with both simulated and experimentally measured data show that the proposed method outperforms the state-of-the-art phaseless inverse scattering method.

Index Terms— phaseless inverse scattering, nonconvex optimization, nonlinear forward model, phase retrieval, total variation regularization.

1. INTRODUCTION

Inverse scattering problems use the scattered wave measurements from a bounded medium to estimate the spatial profile of an object. Inverse scattering has several applications, including, but not limited to, diffraction tomography, coherence tomography, digital holography, microscopy and subsurface radar [1–5]. Most of the traditional methods addressing this problem have considered linear forward models that enable an efficient convex formulation of the inverse problem by neglecting multiple scattering. However, these linear models tend to be highly inaccurate in high contrast settings or when the object size is large compared to the wavelength of the incident wave [6, 7]. These observations have sparked interest in nonlinear formulations that provide a more accurate representation of the physical setup by modeling multiple scattering and facilitate imaging in high contrast settings [8, 9].

In this context, a very interesting and widely applicable problem is recovery from phaseless measurements, i.e., lacking phase information of the measured scattered wave. Thanks to recent advances in the phase retrieval literature, this problem has gained renewed attention and importance. Imaging with phaseless measurements occurs in and has been explored in a variety of applications, including Fourier ptychographic microscopy [10–12], and optical diffraction tomography [13–15], among others [16–19]. The common approach in all those applications is alternating minimization, i.e., methods that alternates between phase estimation (using phase retrieval techniques) and the inversion problem (based on the estimated phase). This is the most popular approach in practical problems.

There exist other phase retrieval approaches, not based on alternating minimization, that are less effective in practice. For example, Wirtinger Flow [20] and PhaseMax [21] exploit a good initialization or initial guess to determine a solution. They enjoy performance guarantees when the forward model operator is a matrix with independent and identically distributed (i.i.d.) Gaussian entries. However, their empirical performance for the inverse scattering problem, where the forward model is nonlinear and structured, is poor in our experiments. Alternatively, PhaseLift [22, 23] performs phase retrieval in a lifted higher dimensional space, where the resulting optimization problem is convex if the forward model operator is linear. Theoretical performance guarantees for PhaseLift have been provided when the forward model matrix is i.i.d. Gaussian [22] or discrete Fourier transform (DFT) with random masks [23]. While we had some limited success with PhaseLift in our experiments for inverse scattering problems, the computational cost is high and makes image priors difficult to impose in the lifted space.

In this paper, we propose a new formulation of the nonlinear forward model for inverse scattering in the presence of phaseless measurements. Our formulation decouples the unknown object and the unknown phase. The decoupling allows us to design an accelerated proximal gradient optimization procedure, which resembles fast iterative shrinkage-thresholding algorithm (FISTA) [24], to jointly optimize over both unknowns. This is in contrast to most existing techniques that are based on alternating minimization. One advantage of the joint optimization scheme over the alternating minimization scheme that we have observed in our experiments is that the convergence and reconstruction quality of

ML did this work while an intern at MERL.

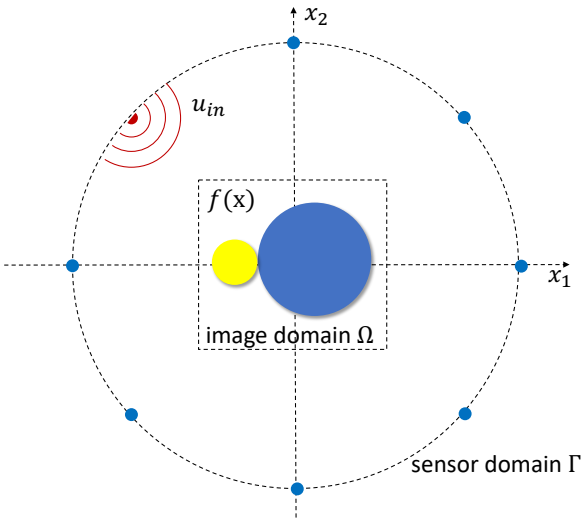

Fig. 1: Imaging setup for phaseless inverse scattering.

the joint optimization scheme is less sensitive to optimization parameters, and consequently less manual tuning is required. Moreover, we solve the problem directly in the image space (as opposed to a lifted space), which circumvents the problem of high computational cost and allows us to conveniently incorporate image priors.

The rest of the paper is organized as follows. In the next section we describe the phaseless inverse scattering problem and our proposed formulation. Section 3 details our proposed joint recovery algorithm PISTA. In Section 4 we validate the performance of our method on both simulated and real data. We discuss our results and conclude in Section 5.

2. PROBLEM FORMULATION

We consider the imaging setup in Fig. 1, where an object of spatial permittivity profile $\epsilon(\mathbf{x})$ is imaged in a bounded domain Ω. Here, $\mathbf{x} \in \mathbb{R}^2$ represents the spatial coordinates in the ambient space. We denote the field due to the incident wave illuminating the object using $u_{in}(\mathbf{x})$ and the field due to the scattered wave, also measured by the sensors positioned outside the bounded domain, as $u_{sc}(\mathbf{x})$. The total field u that exists in the medium is the sum of the two fields: $u(\mathbf{x}) = u_{in}(\mathbf{x}) + u_{sc}(\mathbf{x})$. Moreover, the total field can be related to the incident field and the scattering object through the scalar Lippmann-Schwinger equation [6] as:

$$u(\mathbf{x}) = u_{in}(\mathbf{x}) + \int_{\Omega} g(\mathbf{x}-\mathbf{x}')u(\mathbf{x}')f(\mathbf{x}')d\mathbf{x}', \quad \forall \mathbf{x} \in \mathbb{R}^2,$$

where $f(\mathbf{x}) = k^2(\epsilon(\mathbf{x}) - \epsilon_b)$ represents the scattering potential, ϵ_b denotes the permittivity of the background and $k = 2\pi/\lambda$ is the wavenumber in vacuum. Moreover, $g(\mathbf{x}) = \frac{j}{4}H_0^{(1)}(k_b\|\mathbf{x}\|)$ is the free-space Green's function in 2D, with $H_0^{(1)}$ representing the zero-order Hankel function of the first kind, $k_b = k\sqrt{\epsilon_b}$ representing the background wavenumber, and $\|\cdot\|$ denoting the Euclidean norm.

The (ideal) discretized system for our setup can be expressed as:

$$\begin{aligned} \widehat{\mathbf{y}} &= \mathbf{H}\text{diag}(\mathbf{u})\mathbf{f} \\ \mathbf{u} &= \mathbf{u}_{in} + \mathbf{G}\text{diag}(\mathbf{f})\mathbf{u}, \end{aligned} \tag{1}$$

where $\mathbf{f} \in \mathbb{R}^N$, $\mathbf{u} \in \mathbb{C}^N$, and $\mathbf{u}_{in} \in \mathbb{C}^N$ are samples of $f(\mathbf{x})$, $u(\mathbf{x})$ and $u_{in}(\mathbf{x})$, respectively, obtained at N equispaced points in the domain Ω. Moreover, $\text{diag}(\mathbf{f})$ represents a diagonal matrix with $\mathbf{f}$ on its main diagonal, and $\widehat{\mathbf{y}} \in \mathbb{C}^M$ represents the scattered wave observed in the sensor domain Γ. The matrix $\mathbf{H} \in \mathbb{C}^{M\times N}$ in (1) is a mapping from the image domain to the sensor domain, as defined by discretizing the continuous Green's function $g(\mathbf{x}-\mathbf{x}')$ for $\mathbf{x} \in \Gamma$ and $\mathbf{x}' \in \Omega$. Similarly, the matrix $\mathbf{G} \in \mathbb{C}^{N\times N}$ is the mapping within the image domain, as defined by discretizing the Green's function $g(\mathbf{x}-\mathbf{x}')$ for $\mathbf{x}, \mathbf{x}' \in \Omega$.

If the measurement system is phaseless, only the magnitude of the scattered wave is recorded. Thus, the acquired data (in the absence of noise) can be expressed using (1) as:

$$\begin{aligned} \mathbf{y} &= |\mathbf{H}\text{diag}(\mathbf{u})\mathbf{f}| \\ \mathbf{u} &= \mathbf{u}_{in} + \mathbf{G}\text{diag}(\mathbf{f})\mathbf{u}, \end{aligned} \tag{2}$$

where $\mathbf{y} \in \mathbb{R}^M_{\geq 0}$ represents the magnitude of the scattered wave $\widehat{\mathbf{y}}$ observed in the sensor domain Γ. We model the unknown phase of the scattered wave through a complex phase-only vector $\mathbf{p} \in \mathbb{C}^M$, i.e., $\widehat{\mathbf{y}} = \mathbf{y} \odot \mathbf{p}$, where $\odot$ denotes element-wise product. Thus, phaseless observations satisfy $\mathbf{y} \odot \mathbf{p} = \mathbf{H}\text{diag}(\mathbf{f})\mathbf{u}$. In the presence of noise, (2) can be expressed as:

$$\begin{aligned} \text{diag}(\mathbf{y})\mathbf{p} &= \mathbf{H}\text{diag}(\mathbf{u})\mathbf{f} + \mathbf{e} \\ \mathbf{u} &= \mathbf{u}_{in} + \mathbf{G}\text{diag}(\mathbf{f})\mathbf{u}, \end{aligned} \tag{3}$$

where $\mathbf{e} \in \mathbb{C}^M$ represents the noise. Our main objective is to estimate the unknown object $\mathbf{f}$ and the unknown phase $\mathbf{p}$ given the phaseless observations $\mathbf{y}$ and the incident wave $\mathbf{u}_{in}$, under the constraints that $\mathbf{f}$ is piecewise constant and that $\mathbf{p}$ is a phase-only vector.

The reformulated model in (3) is nonlinear due to the interdependence of the permittivity contrast $\mathbf{f}$ and the total field $\mathbf{u}$. However, if the total field $\mathbf{u}$ is known, the problem becomes linear because our formulation decouples the unknown phase $\mathbf{p}$ from the unknown image $\mathbf{x}$. In contrast, existing formulations maintain a multiplicative coupling between the unknown phase and the recovered image, necessitating either lifting the problem to a higher dimensional space to convexify it [22] or using alternating minimization to solve the nonconvex formulation [15]. Both approaches have their limitations, as we mentioned in Section 1.

3. PHASELESS RECONSTRUCTION ALGORITHM

By rearranging, we can express (3) as:

$$[\mathrm{diag}(\mathbf{y}),\ -\mathbf{H}\mathrm{diag}(\mathbf{u})]\begin{bmatrix}\mathbf{p}\\ \mathbf{f}\end{bmatrix} = \mathbf{e} \tag{4}$$

$$[\mathbf{I} - \mathbf{G}\mathrm{diag}(\mathbf{f})]\mathbf{u} = \mathbf{u}_{in} \tag{5}$$

The unknown $\mathbf{p}$ and $\mathbf{f}$ in (4) lie in the null space of the matrix $[\mathrm{diag}(\mathbf{y}), -\mathbf{H}\mathrm{diag}(\mathbf{u})]$, which might not be unique. It also includes the trivial all-zero solution. Although the constraint (5) on the total field reduces the size of the solution space, we need to introduce more constraints in order to further resolve the ambiguity. We first observe that the object permittivity contrast is typically piecewise constant in spatial coordinates and that it only takes non-negative values. We impose this model using total variation (TV)-based regularization and a non-negativity constraint. We also observe that through our formulation, we assume $\mathbf{p}$ to be a phase-only complex vector with unit entrywise magnitudes such that $|\mathbf{p}_i| = 1$ for $i = 1, \ldots, M$.

With these additional priors and constraints, phaseless inverse scattering requires solving the following optimization:

$$\begin{aligned}\min_{\substack{\mathbf{p}\in\mathbb{C}^M\\ \mathbf{f}\in\mathbb{R}^N}}\ & \frac{1}{2}\left|\left|[\mathrm{diag}(\mathbf{y}),\ -\mathbf{H}\mathrm{diag}(\mathbf{u})]\begin{bmatrix}\mathbf{p}\\ \mathbf{f}\end{bmatrix}\right|\right|_2^2 + \lambda\,\mathrm{TV}(\mathbf{f}) \\ \text{s.t.}\quad & [\mathbf{I} - \mathbf{G}\mathrm{diag}(\mathbf{f})]\mathbf{u} = \mathbf{u}_{in},\ \mathbf{f} \geq \mathbf{0},\ |\mathbf{p}_i| = 1,\ \forall i,\end{aligned} \tag{6}$$

where $\mathrm{TV}(\mathbf{f}) = \sum_{n=1}^{N}\sqrt{|\mathbf{D}_1\mathbf{f}|^2 + |\mathbf{D}_2\mathbf{f}|^2}$ denotes TV regularization, $\mathbf{D}_i$ represents the discrete difference operator in the i-th spatial dimension, and λ is a regularization parameter.

The objective function in (6) consists of a smooth data fidelity term and a non-smooth regularization term. Objective functions of this kind are well suited for accelerated proximal gradient methods like FISTA [24]. Additionally, since the gradient of the objective depends on one of the constraints, it can be efficiently computed via the adjoint-state method. To solve (6), we propose Algorithm 1, which we call Phaseless Iterative Shrinkage-Thresholding Algorithm (PISTA).

In the algorithm, α represents the step size and $\mathcal{P}_{TV,\lambda,(\cdot)\geq\mathbf{0}}$ denotes the proximal mapping for TV regularization with non-negativity constraints, which admits efficient solutions [25]. Similarly, $\mathcal{P}_{|\cdot|=\mathbf{1}}$ denotes the nonconvex proximal mapping onto the surface of the M-dimensional complex sphere, obtained by scaling each complex entry of a vector to have unit magnitude. Finally, $\nabla_{\mathbf{f}}(\mathbf{f},\mathbf{p})$ and $\nabla_{\mathbf{p}}(\mathbf{f},\mathbf{p})$ denote the components associated with $\mathbf{f}$ and $\mathbf{p}$, respectively, of the gradient $\nabla(\mathbf{f},\mathbf{p})$ of the smooth data fidelity term. The explicit expression for the overall gradient can be found in the following proposition:

Proposition 1. *The* $\mathbf{p}$ *and* $\mathbf{f}$ *components of the gradient of the data fidelity term in* (6) *is equal to:*

$$\nabla_{\mathbf{p}}(\mathbf{f},\mathbf{p}) = -\mathrm{diag}(\mathbf{y})^H\mathbf{r}, \tag{7}$$

Algorithm 1: PISTA — Phaseless Iterative Shrinkage-Thresholding Algorithm

Data: $\mathbf{y}$,$\mathbf{H}$,$\mathbf{G}$,α,λ
$\mathbf{q}_1 = \mathbf{f}_0 = \mathbf{0}$; $\mathbf{s}_1 = \mathbf{p}_0 = \mathbf{1}$;
while *stopping criteria* **do**
  $k = k + 1$;
  $\mathbf{f}_k = \mathcal{P}_{TV,\lambda,(\cdot)\geq\mathbf{0}}\big(\mathbf{q}_k - \alpha\nabla_{\mathbf{f}}(\mathbf{q}_k,\mathbf{s}_k)\big)$;
  $\mathbf{p}_k = \mathcal{P}_{|\cdot|=\mathbf{1}}\big(\mathbf{s}_k - \alpha\nabla_{\mathbf{p}}(\mathbf{q}_k,\mathbf{s}_k)\big)$;
  $t_{k+1} = \frac{1+\sqrt{1+4t_k^2}}{2}$;
  $\mathbf{q}_{k+1} = \mathbf{f}_k + \frac{t_k-1}{t_{k+1}}(\mathbf{f}_k - \mathbf{f}_{k-1})$;
  $\mathbf{s}_{k+1} = \mathbf{p}_k + \frac{t_k-1}{t_{k+1}}(\mathbf{p}_k - \mathbf{p}_{k-1})$;
end
Result: $\widehat{\mathbf{p}}$,$\widehat{\mathbf{f}}$

and

$$\nabla_{\mathbf{f}}(\mathbf{f},\mathbf{p}) = \mathrm{diag}(\mathbf{u})^H(\mathbf{H}^H\mathbf{r} + \mathbf{G}^H\mathbf{w}), \tag{8}$$

respectively, where $\mathbf{r} = [\mathbf{H}\mathrm{diag}(\mathbf{u})\mathbf{f} - \mathrm{diag}(\mathbf{y})\mathbf{p}]$ *is the residual vector,* $\mathbf{A} = \mathbf{I} - \mathbf{G}\mathrm{diag}(\mathbf{f})$*, and* $\mathbf{u}$ *and* $\mathbf{w}$ *are found as solutions of the following linear systems:*

$$\mathbf{A}\mathbf{u} = \mathbf{u}_{in}\ ,\ \ \mathbf{A}^H\mathbf{w} = \mathrm{diag}(\mathbf{f})\mathbf{H}^H\mathbf{r}. \tag{9}$$

Proof. The gradient of the data term with respect to $\mathbf{p}$ can be found trivially through matrix derivatives. The derivative with respect to $\mathbf{f}$ is equal to

$$\nabla_{\mathbf{f}}\left[\frac{1}{2}\left|\left|[\mathrm{diag}(\mathbf{y}),-\mathbf{H}\mathrm{diag}(\mathbf{u})]\begin{bmatrix}\mathbf{p}\\ \mathbf{f}\end{bmatrix}\right|\right|_2^2\right] = \mathbf{J}_{\mathbf{f}}^H\mathbf{r}, \tag{10}$$

where $\mathbf{J}_{\mathbf{f}}$ denotes the Jacobian with respect to $\mathbf{f}$, equal to

$$\mathbf{J}_{\mathbf{f}} = \frac{d}{d\mathbf{f}}(\mathbf{H}\mathrm{diag}(\mathbf{u})\mathbf{f}). \tag{11}$$

Using differentials, this derivative can be determined as:

$$\begin{aligned} d(\mathbf{H}\mathrm{diag}(\mathbf{u})\mathbf{f}) &= \mathbf{H}\mathrm{diag}(\mathbf{u})d\mathbf{f} + \mathbf{H}d(\mathrm{diag}(\mathbf{u}))\mathbf{f} \\ &= \mathbf{H}\mathrm{diag}(\mathbf{u})d\mathbf{f} + \mathbf{H}\mathrm{diag}(\mathbf{f})d\mathbf{u}, \end{aligned} \tag{12}$$

where we used the fact that $\mathbf{u}$ is a function of $\mathbf{f}$ and that when taking the differential with respect to only $\mathbf{u}$ we have $d(\mathrm{diag}(\mathbf{u}))\mathbf{f} = d(\mathrm{diag}(\mathbf{u})\mathbf{f}) = d(\mathrm{diag}(\mathbf{f})\mathbf{u}) = \mathrm{diag}(\mathbf{f})d\mathbf{u}$. Moreover, with $\mathbf{u} = \mathbf{A}^{-1}\mathbf{u}_{in}$, we can express the differential of $\mathbf{u}$ as:

$$d\mathbf{u} = -\mathbf{A}^{-1}d\mathbf{A}\mathbf{A}^{-1}\mathbf{u}_{in} = -\mathbf{A}^{-1}d\mathbf{A}\ \mathbf{u}. \tag{13}$$

Finally, the differential of $\mathbf{A}$, is equal to

$$d\mathbf{A} = d(\mathbf{I} - \mathbf{G}\mathrm{diag}(\mathbf{f})) = -\mathbf{G}d(\mathrm{diag}(\mathbf{f})). \tag{14}$$

Therefore, $d\mathbf{A}\mathbf{u} = -\mathbf{G}d(\mathrm{diag}(\mathbf{f}))\mathbf{u} = -\mathbf{G}\mathrm{diag}(\mathbf{u})d\mathbf{f}$. Using all of the differentials, we can express the Jacobian as:

$$\mathbf{J}_{\mathbf{f}} = \mathbf{H}\mathrm{diag}(\mathbf{u}) + \mathbf{H}\mathrm{diag}(\mathbf{f})\mathbf{A}^{-1}\mathbf{G}\mathrm{diag}(\mathbf{u}). \tag{15}$$

Finally, combining (15) with (10) we derive (8). ∎

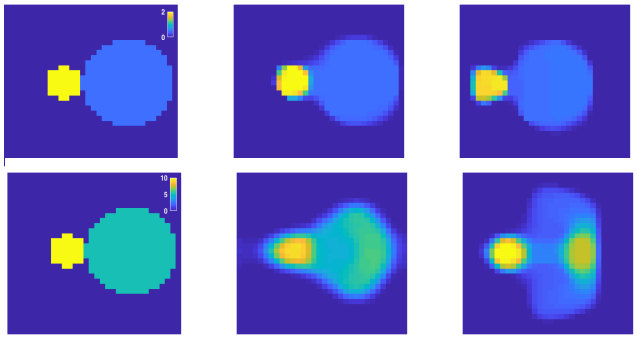

Fig. 2: Comparison of PISTA (center) with ADMM (right) for a simulated objects (left) of different contrast.

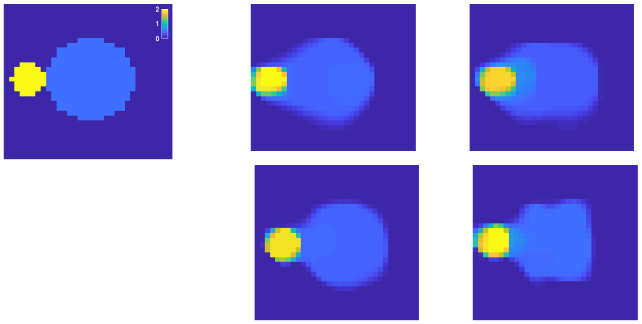

Fig. 3: Comparison of PISTA (center) with ADMM (right) for *FoamDielExtTM* (left) when using single (top row) and multiple (bottom row) frequencies

4. NUMERICAL EXPERIMENTS

To validate our approach, we perform numerical experiments with both simulated and real data. Comparison with the state-of-the-art ADMM based technique for phaseless inverse scattering [15] is provided. The optimization parameters for all methods were manually tuned for optimal performance. The target scene for ADMM is always initialized to all ones, as suggested in [15]. For PISTA, the same initialization can be used but faster convergence is observed empirically for an initialization of all zeros. Additionally, phase estimate of PISTA is also initialized to all ones, i.e., no complex phase.

4.1. Simulated data

In our first set of experiments, we simulated an object of physical size 15cm $\times$ 15cm with two cylinders of different permittivity values. The imaging system comprised of 24 transmitters and 36 receivers, uniformly placed in a circle of radius 1.67m around the object, as shown in Fig. 1. The pixel size was set to 0.4688cm. In the first experiment, the permittivity contrast values of the two cylinders were 2 and 0.45, respectively, and we illuminated the scene with light containing multiple frequencies of wavelengths $\lambda = 6$cm, 7.5cm, 10cm, 15cm, and 30cm. In the second experiment, the permittivity contrast values of the two cylinders were 10 and 5, respectively, and a single wavelength $\lambda = 30$cm was used. Finally, we simulate our synthetic experiments in the absence of noise.

The top row of Fig. 2 shows the results of our first experiment, where the maximum permittivity contrast is 2. In this moderate contrast scenario, PISTA and ADMM have obtained similar performance. The bottom row of Fig. 2 shows the results of our second experiments, where the maximum permittivity contrast is 10. We notice that PISTA visibly outperforms ADMM in this high contrast scenario.

4.2. Real data

In the second set of experiments, we use the the Fresnel Institute public dataset [26], and reconstruct the object *FoamDielExtTM*. In this experiment, eight transmitters and 360 receivers are placed uniformly in a circle of radius 1.67m around the origin. Transmitters are turned on, one at a time, and data from only 241 receivers are used. The remaining 119 receivers closest to the transmitter are kept inactive. We consider a region of 15cm $\times$ 15cm containing the object, and reconstruct the image using both multiple and single frequencies. In both cases we use a pixel size of 0.4688cm. Fig. 3 displays the ground truth and the reconstructed images for PISTA and ADMM for single frequency of wavelength λ =10cm (top row) and for multiple frequencies of wavelengths λ =5cm, 6cm, 7.5cm, 10cm, and 15cm. For both setups, we can see that PISTA results in better reconstructions than ADMM.

5. CONCLUSION

In this paper we reformulated the forward model for nonlinear phaseless inverse scattering. This reformulation decouples the two unknowns, namely the object to be recovered and the unknown phase, which are multiplicatively coupled in earlier approaches. Because of this coupling, existing strategies either use alternating minimization, which is very sensitive to noise and parameter tuning, or lift the problem to a higher dimension, which has impractically large computational costs. In contrast, decoupling the variables allows us to simultaneously optimize over both unknowns efficiently, without lifting. The proposed framework is general and can be used to address other similar problems in phase retrieval.

Of course, this formulation raises a number of open theoretical and practical questions. For example, the problem is nonconvex, lacking global convergence guarantees, and making local guarantees more difficult to derive. However, the decoupling of the unknowns seems to behave better in practice than alternating minimization. In addition, the non-linear effects of the multiple scattering problem makes sample complexity bounds more difficult to obtain.

6. REFERENCES

[1] Y. Sung and R. Dasari, "Deterministic regularization of three-dimensional optical diffraction tomography," *JOSA A*, vol. 28, no. 8, pp. 1554–1561, 2011.

[2] Y. Sung, W. Choi, C. Fang-Yen, K. Badizadegan, R. Dasari, and M. Feld, "Optical diffraction tomography for high resolution live cell imaging," *Optics express*, vol. 17, no. 1, pp. 266–277, 2009.

[3] J. Lim, K. Lee, K. Jin, S. Shin, S. Lee, Y. Park, and J. Ye, "Comparative study of iterative reconstruction algorithms for missing cone problems in optical diffraction tomography," *Optics express*, vol. 23, no. 13, pp. 16 933–16 948, 2015.

[4] V. Lauer, "New approach to optical diffraction tomography yielding a vector equation of diffraction tomography and a novel tomographic microscope," *Journal of Microscopy*, vol. 205, no. 2, pp. 165–176, 2002.

[5] M. Bronstein, A. M. Bronstein, M. Zibulevsky, and H. Azhari, "Reconstruction in diffraction ultrasound tomography using nonuniform fft," *IEEE transactions on medical imaging*, vol. 21, no. 11, pp. 1395–1401, 2002.

[6] M. Born and E. Wolf, *Principles of Optics*, 7th ed. Cambridge Univ. Press, 2003, ch. Scattering from inhomogeneous media, pp. 695–734.

[7] B. Chen and J. Stamnes, "Validity of diffraction tomography based on the first born and the first rytov approximations," *Applied optics*, vol. 37, no. 14, pp. 2996–3006, 1998.

[8] E. Soubies, T.-A. Pham, and M. Unser, "Efficient inversion of multiple-scattering model for optical diffraction tomography," *Optics express*, vol. 25, no. 18, pp. 21 786–21 800, 2017.

[9] Y. Ma, H. Mansour, D. Liu, P. Boufounos, and U. Kamilov, "Accelerated image reconstruction for nonlinear diffractive imaging," in *2018 IEEE International Conference on Acoustics, Speech and Signal Processing (ICASSP)*. IEEE, 2018, pp. 6473–6477.

[10] L. Bian, J. Suo, G. Zheng, K. Guo, F. Chen, and Q. Dai, "Fourier ptychographic reconstruction using wirtinger flow optimization," *Optics express*, vol. 23, no. 4, pp. 4856–4866, 2015.

[11] L. Yeh, J. Dong, J. Zhong, L. Tian, M. Chen, G. Tang, M. Soltanolkotabi, and L. Waller, "Experimental robustness of fourier ptychography phase retrieval algorithms," *Optics express*, vol. 23, no. 26, pp. 33 214–33 240, 2015.

[12] Y. Zhang, W. Jiang, L. Tian, L. Waller, and Q. Dai, "Self-learning based fourier ptychographic microscopy," *Optics express*, vol. 23, no. 14, pp. 18 471–18 486, 2015.

[13] M. Maleki, A. Devaney, and A. Schatzberg, "Tomographic reconstruction from optical scattered intensities," *JOSA A*, vol. 9, no. 8, pp. 1356–1363, 1992.

[14] M. Maleki and A. Devaney, "Phase-retrieval and intensity-only reconstruction algorithms for optical diffraction tomography," *JOSA A*, vol. 10, no. 5, pp. 1086–1092, 1993.

[15] T.-A. Pham, E. Soubies, A. Goy, J. Lim, F. Soulez, D. Psaltis, and M. Unser, "Versatile reconstruction framework for diffraction tomography with intensity measurements and multiple scattering," *Optics express*, vol. 26, no. 3, pp. 2749–2763, 2018.

[16] T. Ralston, A. Marks, P. Carney, and S. Boppart, "Inverse scattering for optical coherence tomography," *JOSA A*, vol. 23, no. 5, pp. 1027–1037, 2006.

[17] D. Liu, U. S. Kamilov, and P. T. Boufounos, "Compressive tomographic radar imaging with total variation regularization," in *2016 4th International Workshop on Compressed Sensing Theory and its Applications to Radar, Sonar and Remote Sensing (CoSeRa)*. IEEE, 2016, pp. 120–123.

[18] M. Leigsnering, F. Ahmad, M. Amin, and A. Zoubir, "Multipath exploitation in through-the-wall radar imaging using sparse reconstruction," *IEEE Transactions on Aerospace and Electronic Systems*, vol. 50, no. 2, pp. 920–939, 2014.

[19] L. Tian, N. Loomis, J. Domínguez-Caballero, and G. Barbastathis, "Quantitative measurement of size and three-dimensional position of fast-moving bubbles in air-water mixture flows using digital holography," *Applied optics*, vol. 49, no. 9, pp. 1549–1554, 2010.

[20] E. J. Candès, X. Li, and M. Soltanolkotabi, "Phase retrieval via wirtinger flow: Theory and algorithms," *IEEE Transactions on Information Theory*, vol. 61, no. 4, pp. 1985–2007, 2015.

[21] T. Goldstein and C. Studer, "Phasemax: Convex phase retrieval via basis pursuit," *IEEE Transactions on Information Theory*, vol. 64, no. 4, pp. 2675–2689, 2018.

[22] E. J. Candès, T. Strohmer, and V. Voroninski, "Phaselift: Exact and stable signal recovery from magnitude measurements via convex programming," *Communications on Pure and Applied Mathematics*, vol. 66, no. 8, pp. 1241–1274, 2013.

[23] E. J. Candès, X. Li, and M. Soltanolkotabi, "Phase retrieval from coded diffraction patterns," *Applied and Computational Harmonic Analysis*, vol. 39, no. 2, pp. 277–299, 2015.

[24] A. Beck and M. Teboulle, "A fast iterative shrinkage-thresholding algorithm for linear inverse problems," *SIAM journal on imaging sciences*, vol. 2, no. 1, pp. 183–202, 2009.

[25] ——, "Fast gradient-based algorithms for constrained total variation image denoising and deblurring problems," *IEEE transactions on image processing*, vol. 18, no. 11, pp. 2419–2434, 2009.

[26] J. Geffrin, P. Sabouroux, and C. Eyraud, "Free space experimental scattering database continuation: experimental set-up and measurement precision," *inverse Problems*, vol. 21, no. 6, p. S117, 2005.